Multiple photoionization and fragmentation of C_{60} in the 18–280-eV range

P. N. Juranić,[1,*] D. Lukić,[2,†] K. Barger,[3] and R. Wehlitz[1,‡]
[1]*Synchrotron Radiation Center, University of Wisconsin–Madison, Stoughton, Wisconsin 53589, USA*
[2]*Columbia Astrophysics Laboratory, Columbia University, New York, New York 10027, USA*
[3]*Western Washington University, Bellingham, Washington 98225, USA*
(Received 4 January 2006; revised manuscript received 7 February 2006; published 3 April 2006)

We examined the relative ionization and fragmentation probabilities of C_{60} after excitation by monochromatized synchrotron radiation in the energy range of 18–280 eV. The energy dependence of the relative cross sections of C_{60}^{q+} ($q=1-4$) and the associated fragments C_{60-2n}^{q+} ($n=1-6$ for $q=2,3$ and $n=1,2$ for $q=4$) are analyzed. We present the ionization and appearance energies for those ions and fragments as well as the partial cross sections for the C_{60} ions.

DOI: 10.1103/PhysRevA.73.042701 PACS number(s): 33.80.Eh, 36.40.Qv, 61.48.+c

I. INTRODUCTION

Buckminsterfullerene, C_{60}, is of scientific interest because it is an exceptionally stable and symmetric cluster with a low sublimation temperature that allows us to study large clusters in gas phase. Observing the behavior of C_{60} after ejecting one or more electrons by photon impact could give us great insight into the multiple-photoionization process of other clusters, and will increase our knowledge about C_{60} clusters.

Earlier studies have extensively explored the C_{60}^{2+} ionization threshold region [1–3] between 18 and 45 eV. Aksela *et al.* [4] and Karvonen *et al.* [5] investigated C_{60} in the higher photon energy range of 280–340 eV near the *K* shell, while Reinköster has explored the intermediate energy region between 26 and 130 eV [6]. Recently, we have investigated the double-photoionization process of C_{60} from threshold to 280 eV, which is published elsewhere [7]. However, multiple photoionization and fragmentation over the full photon energy range from the double-ionization threshold to the *K* shell has not been covered experimentally, with a notable gap in the 130–280-eV region. The present study improves on previous measurements of the double-, triple-, and quadruple-ionization threshold regions, while also bridging the gap between the low and high photon energies. Moreover, we present new data on the C_{60}^{q+} ($q=1-4$) ionization energies and cross sections.

Finally, although the amount of data for ionization and fragmentation of C_{60} by electron impact is large [8–14], there are less fragmentation data available for photoionization. The existence of $C_{58,56}^{2+}$ has been observed in the 60–120-eV range [1] and of C_{52}^{+} at 41 eV [3]. Further studies have observed $C_{58,56,54}^{+}$ ions and double-ionized C_{60-2n} ($n=1-5$) fragments in the 26–130-eV range [6]. None of these papers show higher charge states of these fragments, nor do they present the corresponding appearance energies. Our measurements in the 18–280-eV region presented here show the presence of doubly, triply, and quadruply charged C_{60-2n} ($n=1-6$) fragments along with their appearance energies obtained through single-photon ionization and ion time-of-flight (TOF) spectrometry.

II. EXPERIMENT

A. Beamlines

The data were obtained through a series of experiments performed at the Aladdin Storage Ring at the Synchrotron Radiation Center (SRC) in Stoughton, WI (U.S.A.). The first experiment was performed on the Undulator 4 m Normal Incidence Monochromator (U1 NIM) [15] using an energy range of 18–40 eV with an energy resolution of 15 meV at 25 eV. We had found that stray light affected the data at higher energies (>35 eV), and thus restricted our data to the region between just below the double-ionization threshold (19 eV) and 35 eV. The data were acquired in 0.1 eV steps in the 19–22 eV region, in 0.2 and 0.25 eV steps in the 22–26-eV region, and in 0.5 eV steps beyond that. The acquisition times depended on the photon energy, and they ranged from up to an hour near threshold to five min in the midrange energies, and up to half an hour near 35 eV. Most data points were measured at least twice and the measured values were averaged.

The second experiment was performed on the 6 meter Toroidal Grating Monochromator (6 m-TGM) [16] which has an energy range of 8–200 eV with an energy resolution between 54 meV at lower energies and 0.3 eV at higher energies. Second order light was present at the lower energies unless suppressed by an appropriate filter. In the case of the 6 m-TGM we had used Al and Si_3N_4 filters for the 36–70 eV and 70–100-eV range, respectively. Thus, data below 36 eV were not taken. Similarly, data above 180 eV were affected by stray light and useful data were limited to the 36–180-eV range. The acquisition times were, on average, 15 minutes to half an hour and were taken in 2–5-eV steps. The measurements were done typically twice at each photon energy.

The third experiment was performed on the Wadsworth Normal Incidence Monochromator beamline [17] that has an energy range of 7.8–45 eV with an energy resolution of

*Electronic address: pnjuranic@wisc.edu
†On leave from Institute of Physics, P.O. Box 57, 11001 Belgrade, Serbia and Montenegro.
‡Electronic address: wehlitz@src.wisc.edu

40 meV at 20 eV. There was no second-order or stray light present, and the data were taken in the 19–45-eV range. The acquisition times were typically 30 min long, taken in 0.25–0.5-eV steps.

The fourth and final experiment was done on the Mark II Grasshopper [18] beam line that has an energy range of 40–800 eV with a resolution of 0.7 eV at 170 eV. The measurements were taken over an energy range of 56–280 eV in 5 eV intervals with an average acquisition time of about half an hour. Aluminum, Si_3N_4, and carbon filters were used to suppress second-order light in the 56–70-eV, 70–100-eV, and 150–280-eV ranges, respectively, while the beamline itself had no measurable second-order light in the 100–150 eV region. The measurements were done typically twice at each energy.

Because of the good resolution of the beam lines near the double-ionization threshold and the lack of a need for better resolution at higher energies, the slits on the beam lines were kept open for most of the spectra taken. The energy resolutions mentioned above are for the slit settings used on these beam lines.

B. Experimental apparatus

The monochromatic photon beam passed through a differential pumping stage which also contained our filter arrays. The capillary connecting the differential pumping stage to the main chamber was electrically insulated from the rest of the chamber, and the chamber was aligned so that the photocurrent created on the capillary was minimized (usually at about 100 pA or less) to ensure good alignment with the photon beam. The capillary was then also biased to prevent electrons, created on the capillary's surface by the photon beam, from entering the main chamber and ionizing the C_{60}, ensuring that only *photo*ionization is taking place.

The photon beam intersected the C_{60} vapor that emerged from a resistively heated oven in the main chamber. The oven temperature was typically 375 °C, applying a 0.8 A current and a 10.5–10.6 V potential across the twin core heating wire. While all previous papers in the literature reported performing their experiments at temperatures that were considerably higher [1,2,4–6,8–14], we had no problem in obtaining excellent and very strong peaks at temperatures just above 350 °C. Considering that the vapor pressure of C_{60} is already about 7×10^{-4} Pa at room temperature, it does not seem necessary to use a higher temperature to achieve a vapor density needed for the experiment, given a sufficiently wide oven nozzle for the vapor to sublime through. As Fig. 1 shows, once a C_{60} molecule in the vapor became photoionized, it was extracted by a pulsed electric field across the interaction region, and then accelerated into the drift tube. The electric field was pulsed every 45 μs for 4.5 μs. At the end of the drift tube was a Z stack microchannel-plate (MCP) detector which recorded the ion impacts. By measuring the ion's flight time, we obtained a TOF ion-yield spectrum for C_{60} and fragment ions [19]. Because we did not observe any influence of thermal electrons on the spectra, which could have contaminated the interaction region, we did not bias the oven but left it grounded.

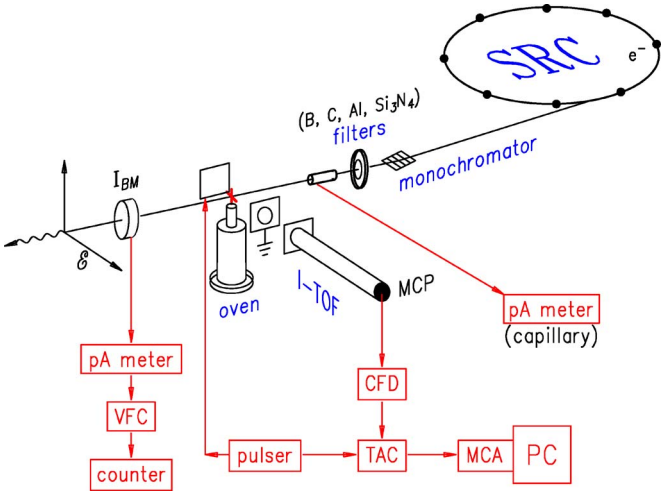

FIG. 1. (Color online) Sketch of the experimental setup.

C. Experimental parameters

The C_{60} used in the experiment was a 99.5% pure powder. During the experiment, the pressure in the chamber was never higher than 1×10^{-8} mbar, and was usually in the $3-5\times10^{-9}$ mbar region. Because of the large mass of the C_{60} molecules there were no overlaps with ionization peaks of common contaminants in vacuum chambers (N_2, H_2O, etc). Even so, our contaminant peaks were small, giving us excellent spectra, as shown in Fig. 2. While the resolution was good enough to separate the doubly charged fragments, it could not be reliably done for the singly charged ones. Therefore, all our ratios are based on the total areas of all singly charged fragments added together.

Neon and argon gas was used during the experiments for photon energy calibration and for the derivation of partial cross sections of the fragments and ions. In addition, we also used Xe and Kr to calibrate the energy of the Mark II Grasshopper beamline. The calibration gases were kept at a steady pressure for the duration of their measurements via a regulator and a needle valve.

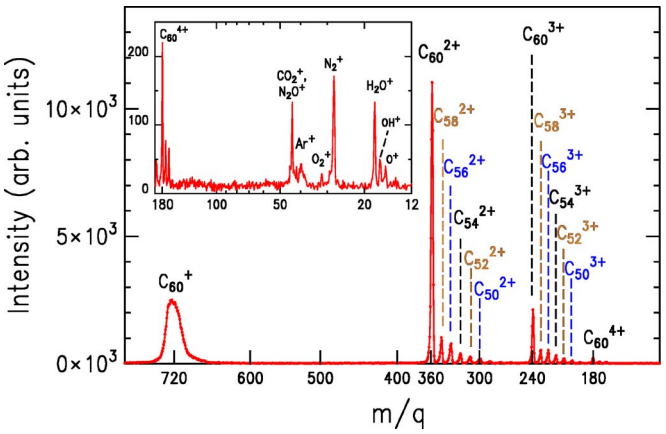

FIG. 2. (Color online) C_{60} time-of-flight spectrum taken at a photon energy of 210 eV on a nonlinear mass-to-charge ratio scale. Note that the ion and fragment peaks of the residual gases, shown in the inset, are small and do not affect the areas of the C_{60} peaks.

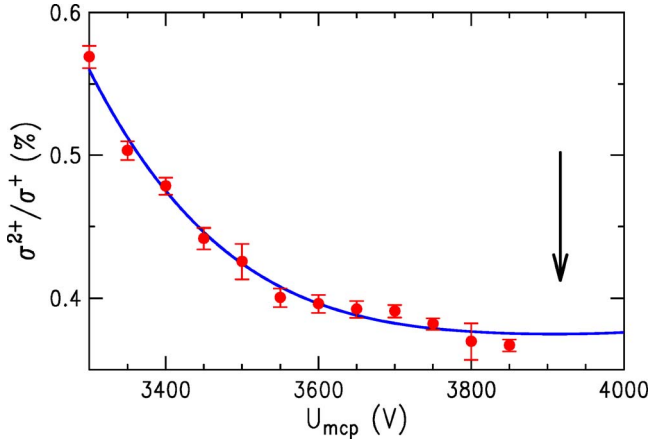

FIG. 3. (Color online) The C_{60}^{2+}/C_{60}^{+} ratio taken at 23 eV as a function of the front MCP voltage. The best MCP voltage corresponds to the minimum value which was extracted via a polynomial fit (solid line). The minimum of the polynomial fit is marked with an arrow and corresponds to 3915 V.

The preamplified (×10) MCP pulse was processed by a constant-fraction discriminator (CFD). The threshold of the CFD was set to a level of 28 mV (its lowest setting) to ensure that there was no difference in the detection efficiencies between the singly and doubly charged ions. Because the C_{60}^{+} count rate decreases faster with increasing CFD threshold, our setting of the CFD to the lowest value ensured we would not be measuring relative ratios that were too high. The only disadvantage in setting the threshold to such a low level is an increased background in the spectra but it did not pose a problem here.

We also looked at the C_{60}^{2+}/C_{60}^{+} ratios as a function of MCP voltage on the front plate. Figure 3 shows that this ratio decreases as the MCP voltage increases due to the different detection efficiencies of differently charged ions. Although we did not apply in the first two experiments the ideal MCP voltage of about 3915 V, we adjusted the few, earlier data by a factor of 1.57 to match the majority of data taken using the most efficient MCP voltage. Note that this adjustment was not done according to the curve in Fig. 3 but was based on the actual data, because we applied the voltage differently to the MCPs. Our earlier measurements have been repeated at the same photon energies with the correct MCP voltage, and the correction factor applied here is the average factor between the two sets of ratios.

Finally, we also studied the possible influence of the oven temperature on the relative cross sections of multiple-ionized C_{60}. We tested this for temperatures between 210 °C and 380 °C by controlling the heating wire current and did not find a dependence of the relative cross section on the temperature of the oven. We kept the temperature constant at 375 °C during the experiments.

III. DATA ANALYSIS

In order to determine the photon energy dependence of the relative cross sections of C_{60}, we took TOF spectra over a range of photon energies. The areas of the C_{60} ion and fragment peaks were either modeled with an asymmetric Voigt profile and their areas extracted, or directly numerically integrated. The reason for not numerically integrating all peaks is the narrow spacing of the fragments at higher energies as shown in Fig. 4. Nevertheless, the areas of the ion peaks could be determined reliably. At some photon energies the spectra were taken repeatedly and only the average value is shown resulting in a smaller error bar.

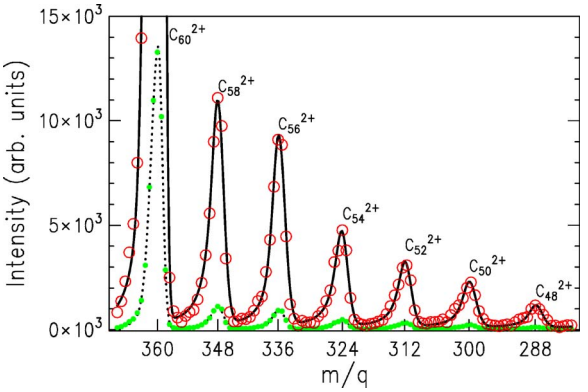

FIG. 4. (Color online) A typical example of a Voigt-profile fit applied to our ion-yield spectrum in the region of doubly charged ions taken at 255 eV. The fit curve (solid line) and data points (open circles) are both multiplied by 10 relative to the dotted line and filled circles, respectively.

We applied an energy correction to the photon energies for those beam lines whose calibration data demonstrated an energy offset larger than the energy resolution. We calibrated the photon energy by observing the Ar $3s\rightarrow5p$ resonance at 27.993 eV [20], the Ar $2p_{3/2}\rightarrow4s$ resonance at 244.39 eV [21], the Ne $2s\rightarrow3p$ resonance at 45.5442 eV [22], the Xe $4d\rightarrow6p$ resonance at 65.110 eV [21], and the Kr $3d\rightarrow5p$ resonance at 91.2 eV [21] via an ion-yield scan across the resonance regions. The corrections of the photon energy were assumed to be a constant offset in wavelength for all the spectra taken in the region of interest.

All our ratios were calculated using the area of all C_n^{+} ($n\leqslant60$) peaks. As mentioned earlier, our resolution could not reliably differentiate between C_{60}^{+} and the nearest singly charged fragment peaks, so we used the sum of all single-ionized ion areas for our calculations. Note that no fragmentation takes place below 47 eV [6].

The relative C_{60}^{+} cross sections were calculated at each photon energy $h\nu$ by dividing the areas of single-ionized C_{60}, $C(h\nu)$, with the areas of either single-ionized Ar or Ne, $A(h\nu)$ and multiplying these ratios with the known cross sections for Ar or Ne [23,24], $R(h\nu)$. In order to derive the absolute partial cross sections for producing C_{60}^{+}, we normalized our relative cross sections by a factor N such that the sum of our single- and double-photoionization cross sections matches the photoabsorption cross section at 40.8 eV derived by Berkowitz [25]. In short, we used the formula

$$\sigma^{+}(h\nu) = N\frac{C(h\nu)}{A(h\nu)}R(h\nu) \tag{1}$$

to derive the absolute cross sections $\sigma^{+}(h\nu)$. It is worth noting that this method does not require a measurement of the

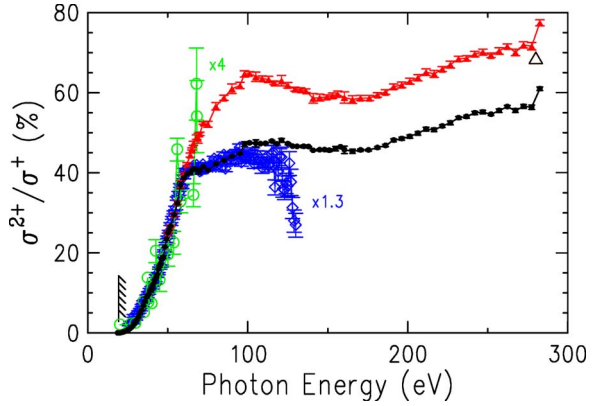

FIG. 5. (Color online) Double-to-single photoionization cross-section ratio as a function of photon energy. The filled triangles represent the relative cross sections of the sum of all double-ionized fragments peak areas. The filled circles represent just the C_{60}^{2+} peak, the open circles represent experimental results of Drewello *et al.* [1] scaled by a factor of 4, while the open diamonds represent the results of Reinköster *et al.* [6] scaled by a factor of 1.3. A 280 eV point from the results of Aksela *et al.* [4] and Karvonen *et al.* [5] is shown as an open triangle.

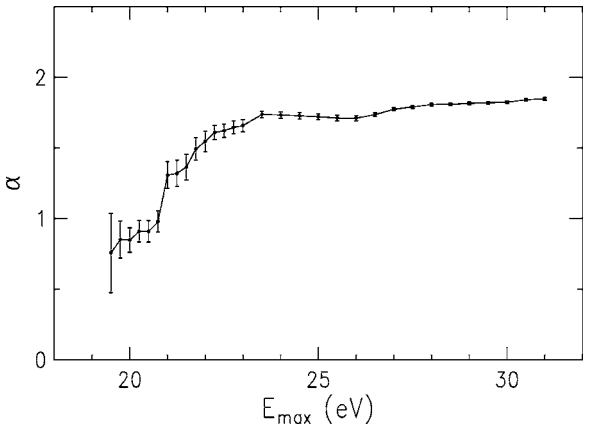

FIG. 6. The Wannier exponent α as a function of the upper limit E_{max} of the fit range using the formula $\sigma^{2+}/\sigma^{+} \propto (h\nu - 19.0)^{\alpha}$ where $h\nu$ is the photon energy in eV. The minimum of the fit range is the double-ionization threshold of 19.00 eV.

photon flux. However, it assumes that the density of the Ar (Ne) and C_{60} gas does not change with time.

In order to derive the partial cross sections σ^q for producing higher charge states q ($q=2-4$), we used the formula

$$\sigma^q(h\nu) = \sigma^+(h\nu)C^q(h\nu)/C(h\nu). \quad (2)$$

Here, $C(h\nu)$ and $C^q(h\nu)$ are the areas of the C_{60}^{+} peak and the C_{60}^{q+} peak, respectively.

IV. RESULTS AND DISCUSSION

A. Doubly charged ions

Figure 5 shows both the double-to-single ionization cross-section ratios of the sum of all fragments, as well as just that of the C_{60}^{2+} ion. Shown alongside our data are previously published ratios of Drewello *et al.* [1], Reinköster *et al.* [6], Aksela *et al.* [4], and Karvonen *et al.* [5] which qualitatively agree with our data. However, the ratios of Refs. [1,6] are multiplied by different factors as indicated in the figure. Note that the ratio at 280 eV of Karvonen *et al.* [5] agrees with our ratio very well without any scaling. The energy dependence of the data from Drewello *et al.* [1] agrees well with our data at energies smaller than 50 eV, but their large error bars make a true comparison difficult. The data points of Reinköster *et al.* [6] agree with our data (except for the scaling) quite well up to 100 eV at which point they tend to be systematically lower, possibly due to stray light present at higher energies. Our points were taken with different gratings and different filters on different beamlines, creating an occasional small kink in the ratio when the filter or grating was changed. The C_{60}^{2+} threshold of 19.00(7) matches most of the previous data for the double-ionization energy measured by both photoionization and electron-impact ionization as listed in Table I.

To check whether the Wannier power law [26] can be applied to the relative cross section near threshold, we performed several power-law fits over a variable range of photon energies, with the lower end of the fit always being the threshold (19.00 eV). As the upper limit of the fit range increases, the value of the exponent α for the power-law fit goes up from its initial value of 0.73 to about 1.7, where it becomes almost constant (Fig. 6). The theoretical value of $\alpha=1.056$ is obviously not reached for our near-threshold data, perhaps because C_{60}^{2+} is strongly polarized. However,

TABLE I. Ionization and appearance energies of C_{60}^{2+} and its double-ionized fragments compared to experimental values observed in previous investigations. n denotes the number of carbon atoms in the ion.

n	This work	[6]	[14]	[2]	[3]	[8]	[10]	[13]
60	19.00(7)		19.0	19.00(3)	19.5	19	19.1	18.98(25)
58	55.5(8)	59	53.9			54	54.1	
56	60(2)	61	59.8			59.8	59.9	
54	68.8(6)	74	65.1					
52	73(4)	77	71.8					
50	77(1)	86	75.8					
48	80(1)		82.1					

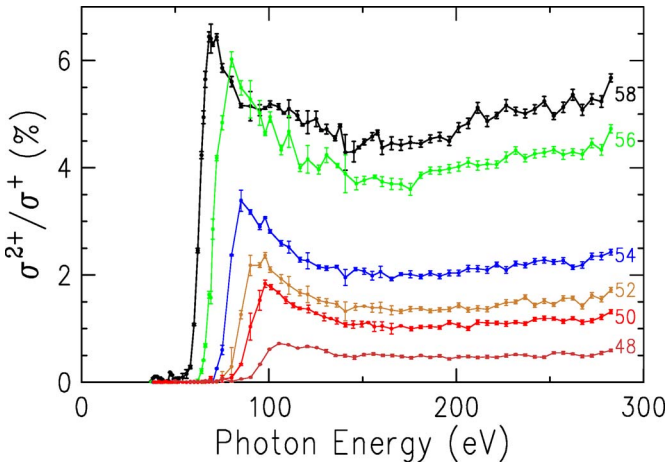

FIG. 7. (Color online) Double-to-single photoionization cross-section ratios of C_n^{2+} fragments for $n=58,56,54,52,50,48$ as a function of photon energy.

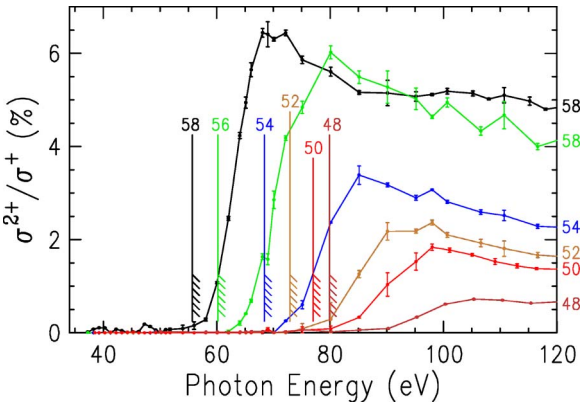

FIG. 8. (Color online) A closeup of Fig. 7 in the appearance energy region of the C_n^{2+} fragments for $n=58,56,54,52,50,48$. The markings show the appearance energies as labeled in the figure. The curves for the different fragments are labeled on the right-hand side of the frame.

if one would get much closer to threshold, the Wannier exponent of 1.056 may be recovered.

A careful look at the double-to-single photoionization ratio reveals a modulation of that ratio [7]. In Fig. 5 the modulation is clearly visible above 90 eV, where one can see a hump, followed by a dip, and then another hump. The ratio is increased at certain excess (kinetic) energies (i.e., photon energy minus double-ionization threshold), where the corresponding de Broglie wavelength of one of the two electrons created in the double-ionization process matches various distances unique to C_{60} molecules. While this enhancement is rather small at lower energies, it becomes larger at higher energies. These distances correspond to the distance between two neighboring carbon atoms, the diameter of the cluster, or the diameter of a hexagon. A detailed discussion of this effect has been published recently [7].

Figure 7 shows the relative cross sections of the doubly charged fragments from their appearance, when C_2 molecules start to break off, up to 280 eV. Note that the relative photoionization cross section of C_{48}^{2+} has not been shown before. The energy dependence of the fragment curves is similar in that they all exhibit a high sloped increase from their appearance energies that abruptly ends with a peak. Beyond the peak, the curves slope down gently, become horizontal, and even rise again slightly. The maxima and appearance energies in the fragments' relative photoionization cross sections appear at successively higher energies as the fragments become smaller.

We used a power-law function fit in the appearance energy region of the double-ionized fragments shown in Fig. 8. We moved up the lower limit of the fit range until the minima became stable in order to reduce the influence that the points below the appearance energies had on the overall fits. In case there were an insufficient number of points for a fit, or the points could not give a reliable fit, we placed the appearance energy in the middle of the appearance region, with error bars that covered the whole region. The appearance energies, along with those of previous papers dealing with both photoionization and electron-impact ionization, are shown in Table I.

B. Triply charged ions

Our triple-photoionization cross-section ratios are shown in Fig. 9 together with the data presented by Reinköster *et al.* [6], showing good qualitative agreement above the threshold energy. Again, as for the double-to-single photoionization ratio, we see a deviation of the two sets of ratios from each other starting at an energy where the triple-ionized fragments begin appearing. However, as Fig. 10 demonstrates, the shapes of the ratio curves do not exhibit a hump followed by a dip, as the double-ionization ratios do. Instead, all of the curves seem to be similar in shape and go up gradually after reaching a plateau region. This energy dependence is similar to the one for the C_{60}^{3+} ratio, which is not the case for the double-ionized fragment ratio.

As in the case of double-ionized fragments, the appearance energies go up from larger to smaller fragments as more carbon dimers (C_2) break off (see Fig. 11). However, the differences between the appearance energies seem to be

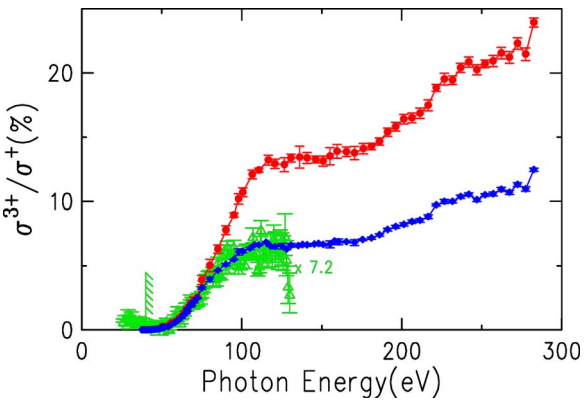

FIG. 9. (Color online) Triple-to-single photoionization ratios as a function of photon energy. The circles represent the cross-section ratios of the sum of all triply charged fragments. The diamonds represent the cross-section ratios of just the C_{60}^{3+} fragment, while the triangles represent the data for the C_{60}^{3+} ratios as presented by Reinköster *et al.* [6], but scaled by a factor of 7.2.

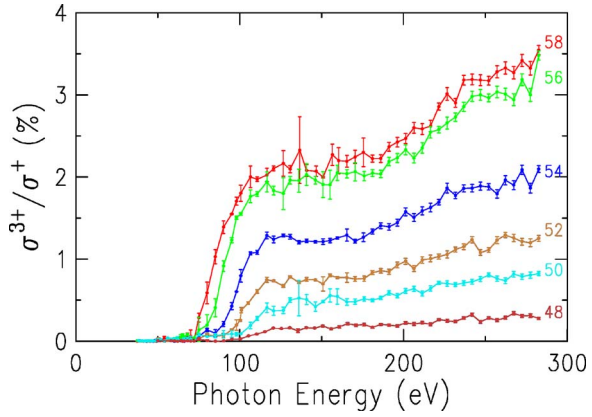

FIG. 10. (Color online) Triple-to-single photoionization ratios of C_n^{3+} fragments for $n=58,56,54,52,50,48$ as a function of photon energy.

smaller for triple-ionized fragments than for double-ionized fragments, and both C_{52}^{3+} and C_{50}^{3+} appear at the same energy, as listed in Table II. The appearance energies were determined by applying a power-law function fit to the threshold region. If there were insufficient points or the fit procedure did not work, the appearance energy was set to the middle of the threshold region, with error bars that cover the whole range where the fragment might have appeared. Although the majority of our appearance energies are lower than those obtained by electron impact [14], our triple-photoionization threshold energy of C_{60} is substantially higher than the one for electron impact. However, our relative cross-section curve for triple-ionized C_{60}, displayed in Fig. 9, agrees qualitatively with the one of Reinköster *et al.* [6], which was also obtained by photoionization.

C. Quadruply charged ions

The highest ionization state of C_{60} that we have reliably observed below the *K* shell is the quadruple-ionization state. We determined the threshold and appearance energies of

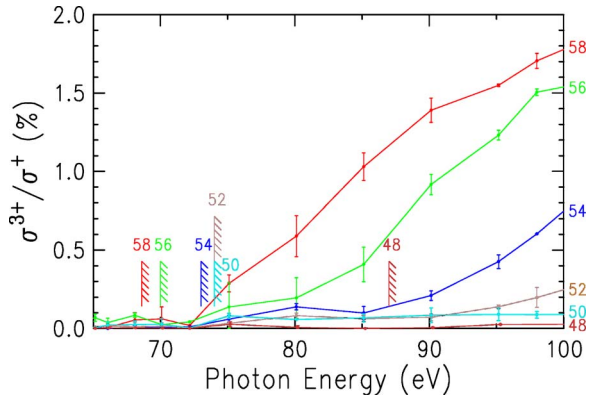

FIG. 11. (Color online) Relative cross sections of triple-ionized fragments C_n^{3+} ($n=58,56,54,52,50,48$) near their appearance energies. The markings show the appearance energies as labeled in the figure. The curves for the different fragments are labeled on the right-hand side of the frame.

TABLE II. Appearance and ionization energies of triply charged ions and fragments compared to experimental values observed in previous investigations. *n* represents the number of carbon atoms in the ion.

n	This work	[14]	[13]	[10]	[8]
60	39.8(5)	35.6	35.8(3)	35.7	35.6
58	68.6(4)	70.3			
56	70(2)	76			
54	73(3)	82.2			
52	74(2)	90.6			
50	74(2)	94.1			
48	87(3)				

C_{60}^{4+}, C_{58}^{4+}, and C_{56}^{4+} that, to our knowledge, has not been done before, neither by photoionization nor by electron-impact ionization. Figure 12 shows the relative cross-section curves of those three ions, as well as the relative cross section of their sum. It is interesting to note that the shapes of the curves have a similar energy dependence.

The appearance energies of the C_{60}^{4+} and the fragments C_{58}^{4+} and C_{56}^{4+} seem to be much more closely spaced than the one for doubly and triply charged fragments. The threshold energy for C_{60}^{4+} was determined to be 69(1) eV. The appearance energies for C_{58}^{4+} and C_{56}^{4+} are approximately at 74(7) eV and 74(9) eV, respectively. The weakness of the quadruple-ionization process in the threshold region makes the determination of a threshold energy particularly difficult, resulting in the large error bars.

D. Partial cross sections

In Fig. 13 the cross sections of singly to quadruply charged C_{60} ions are displayed. We extended the energy range of Reinköster *et al.* [6] to 240 eV as well as more thoroughly explored the double-ionization threshold region

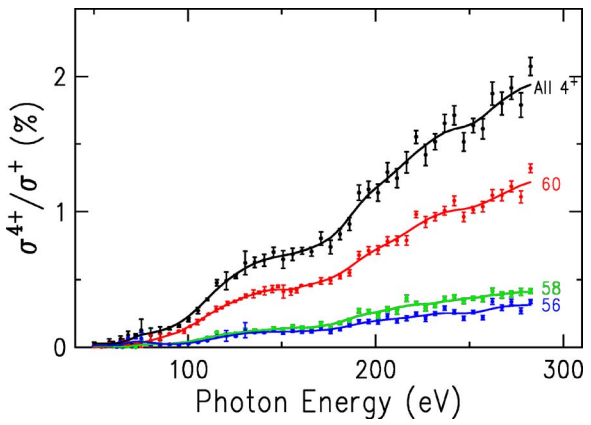

FIG. 12. (Color online) Quadruple-to-single photoionization ratios of C_{60} and its fragments. The top line shows the quadruple-to-single ionization ratio of all quadruply charged fragments. The other data display the ratio for selected masses as indicated in the figure.

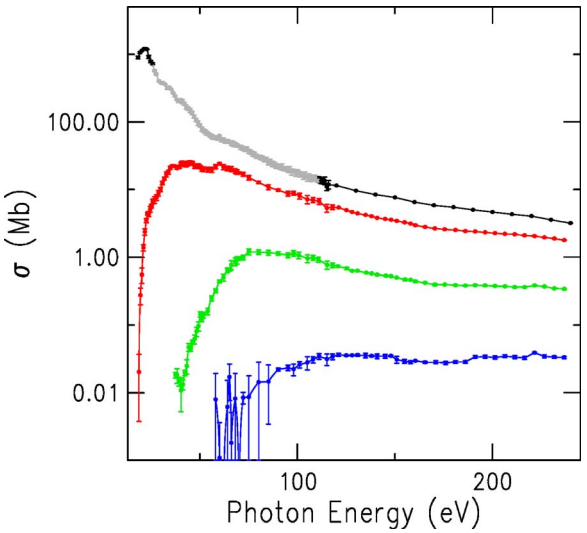

FIG. 13. (Color online) Cross sections of C_{60}^{q+} ions ($q=1-4$). The top line depicts the photoionization cross section of C_{60}^{+}, followed by C_{60}^{2+}, C_{60}^{3+}, and C_{60}^{4+}. The gray data points for C_{60}^{+} in the 26 to 110 eV region are those from Reinköster *et al.* [6].

(19–26 eV). As described above, we put our cross-section data on an absolute scale using the 40.8 eV data point given by Berkowitz [25] in the same manner as in Ref. [6]. The data shown in Fig. 13 are for the C_{60} molecule only and not its fragments, except for the single-ionization cross section, in which case the fragments were not resolved. The error bars shown are based only on the statistical errors of our areas of the C_{60}^{+} and Ne^{+} (or Ar^{+}) peaks. An uncertainty of less than 10% in the Ne and Ar cross section data [23,24] contributes to the systematical error.

As Fig. 13 shows, the ion yield for C_{60}^{+} rises until about 23 eV due to a plasmon resonance [27], at which point it dips down and decreases slowly with increasing energy. The C_{60}^{2+} photoionization cross section rises sharply from its threshold at 19 eV to a high at 32 eV, where it appears to level off before it starts to descend at about 62 eV. Above 100 eV it decreases similarly to the C_{60}^{+} cross section. We observe a similar energy dependence with the triple-photoionization cross section, where a sudden rise of the cross section starting at 39 eV ends at a hump at around 75 eV, at which point the curve begins to descend. The quadruple-photoionization cross section is different as it does not seem to have a marked maximum, nor does it descend as obviously as the cross sections of the other charge states. Instead, it rises until around 115 eV, at which point the photoionization cross section remains almost flat. The error bars for the quadruple-photoionization data are rather large near threshold due to extremely low ion yields for the C_{60}^{4+} state.

V. CONCLUSION

We undertook a comprehensive study of the photoionization and fragmentation of neutral C_{60} molecules between 18 eV and the *K*-shell region at 280 eV. We measured the relative cross sections for all C_{60-2n}^{q+} ions ($n=0-6$ for $q=2,3$ and $n=0-2$ for $q=4$) with respect to the sum of all C_m^{+} ($m=48-60$) and derived the partial cross sections for C_{60}^{q+} ions ($q=1-4$) between 19 and 240 eV. In addition, we have presented the threshold and appearance energies of the above-mentioned fragments and ions. Special mention should be made of the photoionization cross section of C_{60}^{4+}, which, to our knowledge, has not been published before, along with the C_{58}^{4+} and C_{56}^{4+} fragments. Although the higher ($q=3,4$) ionization thresholds do not match with published electron-impact data, they qualitatively match with previously measured photoionization data. Furthermore, our data bridge the gap in the C_{60} photoionization data between 130 and 280 eV, qualitatively agreeing with other relative photoionization cross sections.

ACKNOWLEDGMENTS

The authors wish to thank the staff of the Synchrotron Radiation Center for their excellent support. One of us (D.L.) was partly supported by the Ministry of Science and Environment Protection, Serbia. We thank Dr. Reinköster for sending us his data in numerical form. This work is based upon research conducted at the Synchrotron Radiation Center, University of Wisconsin–Madison, which is supported by the NSF under Grant No. DMR-0084402

[1] T. Drewello, W. Krätschmer, M. Fieber-Erdmann, and A. Ding, Int. J. Mass Spectrom. Ion Process. **124**, R1 (1993).
[2] H. Steger, J. deVries, B. Kamke, W. Kamke, and T. Drewello, Chem. Phys. Lett. **194**, 452 (1992).
[3] R. K. Yoo, B. Ruscic, and J. Berkowitz, J. Chem. Phys. **96**, 911 (1992).
[4] S. Aksela, E. Nõmmiste, J. Jauhiainen, E. Kukk, J. Karvonen, H. G. Berry, S. L. Sorensen, and H. Aksela, Phys. Rev. Lett. **75**, 2112 (1995).
[5] J. Karvonen, E. Nõmmiste, H. Aksela, and S. Aksela, J. Chem. Phys. **106**, 3466 (1997).
[6] A. Reinköster, S. Korica, G. Prümper, J. Viefhaus, K. Godehusen, O. Schwarzkopf, M. Mast, and U. Becker, J. Phys. B **37**, 2134 (2004).
[7] P. N. Juranić, D. Lukić, K. Barger, and R. Wehlitz, Phys. Rev. Lett. **96**, 023001 (2006).
[8] A. Itoh, H. Tsuchida, K. Miyabe, T. Majima, and N. Imanishi, J. Phys. B **32**, 277 (1999).
[9] R. Völpel, G. Hofmann, M. Steidl, M. Stenke, M. Schlapp, R. Trassl, and E. Salzborn, Phys. Rev. Lett. **71**, 3439 (1993).
[10] P. Scheier, D. Hathiramani, W. Arnold, K. Huber, and E. Salzborn, Phys. Rev. Lett. **84**, 55 (2000).
[11] M. S. Baba, T. S. L. Narasimhan, R. Balusubramanian, and C. K. Matthews, J. Phys. Chem. **99**, 3020 (1995).

[12] G. Seifert, R. Gutierrez, and R. Schmidt, Phys. Lett. A **211**, 357 (1996).
[13] A. V. Pogulay, R. R. Abzalimov, S. K. Nasibullaev, A. S. Lobach, T. Drewello, and Y. V. Vasil'ev, Int. J. Mass. Spectrom. **233**, 165 (2004).
[14] P. Scheier, B. Dünser, R. Wörgötter, M. Lezius, R. Robl, and T. D. Märk, Int. J. Mass Spectrom. Ion Process. **138**, 77 (1994).
[15] T. Kubala, M. Bissen, M. Severson, G. Rogers, D. Wallace, M. Thikim, and M. V. Fisher, in Proceedings of the SRI: Eleventh US National Conference AIP Conf. Proc., No. 521, edited by P. Pianetta, J. Arthur, and S. Brennan (AIP, New York, 2000), p. 91.
[16] R. K. Cole, F. K. Perkins, E. L. Brodsky, A. Filipponi, E. Korpella, D. C. Mancini, C. H. Pruett, D. J. Wallace, J. T. Welnak, and F. Zanini, Rev. Sci. Instrum. **60**, 2093 (1989).
[17] J. Bisognano, M. Severson, M. A. Green, G. Rogers, M. Fisher, T. Kubala, and M. Bissen, Nucl. Instrum. Methods Phys. Res. A **467**, 492 (2001).
[18] D. J. Wallace, G. C. Rogers, and S. L. Crossley, Nucl. Instrum. Methods Phys. Res. A **347**, 615 (1994).
[19] R. Wehlitz, D. Lukić, C. Koncz, and I. A. Selin, Rev. Sci. Instrum. **73**, 1671 (2002).
[20] S. L. Sorensen, T. Aberg, J. Tulkki, E. Rachlew-Källne, G. Sundström, and M. Kirm, Phys. Rev. A **50**, 1218 (1994).
[21] G. C. King, M. Tronc, F. H. Read, and R. C. Bradford, J. Phys. B **10**, 2479 (1977).
[22] K. Schulz, M. Domke, R. Püttner, A. Gutiérrez, G. Kaindl, G. Miecznik, and C. H. Greene, Phys. Rev. A **54**, 3095 (1996).
[23] W. F. Chan, G. Cooper, X. Guo, and C. E. Brion, Phys. Rev. A **45**, 1420 (1992).
[24] W. F. Chan, G. Cooper, X. Guo, G. R. Burton, and C. E. Brion, Phys. Rev. A **46**, 149 (1992).
[25] J. Berkowitz, J. Chem. Phys. **111**, 1446 (1999).
[26] G. H. Wannier, Phys. Rev. **90**, 817 (1953).
[27] I. V. Hertel, H. Steger, J. de Vries, B. Weisser, C. Menzel, B. Kamke, and W. Kamke, Phys. Rev. Lett. **68**, 784 (1992).